ground water

Gas-Partitioning Tracer Test to Quantify Trapped Gas During Recharge

by Victor M. Heilweil[1], D. Kip Solomon[2], Kim S. Perkins[3], and Kevin M. Ellett[4]

Abstract

Dissolved helium and bromide tracers were used to evaluate trapped gas during an infiltration pond experiment. Dissolved helium preferentially partitioned into trapped gas bubbles, or other pore air, because of its low solubility in water. This produced observed helium retardation factors of as much as 12 relative to bromide. Numerical simulations of helium breakthrough with both equilibrium and kinetically limited advection/dispersion/retardation did not match observed helium concentrations. However, better fits were obtained by including a decay term representing the diffusive loss of helium through interconnected, gas-filled pores. Calculations indicate that 7% to more than 26% of the porosity beneath the pond was filled with gas. Measurements of laboratory hydraulic properties indicate that a 10% decrease in saturation would reduce the hydraulic conductivity by at least one order of magnitude in the well-sorted sandstone, but less in the overlying soils. This is consistent with in situ measurements during the experiment, which show steeper hydraulic gradients in sandstone than in soil. Intrinsic permeability of the soil doubled during the first six months of the experiment, likely caused by a combination of dissolution and thermal contraction of trapped gas. Managers of artificial recharge basins may consider minimizing the amount of trapped gas by using wet, rather than dry, tilling to optimize infiltration rates, particularly in well-sorted porous media in which reintroduced trapped gas may cause substantial reductions in permeability. Trapped gas may also inhibit the amount of focused infiltration that occurs naturally during ephemeral flood events along washes and playas.

Introduction

Artificial recharge by the spreading of water in surface basins often occurs under an effective field hydraulic conductivity that is lower than the fully saturated hydraulic conductivity. This lower conductivity is caused either by partially saturated conditions and a continuous gas phase or because of trapped gas bubbles as a discontinuous gas phase in an otherwise saturated porous medium (Fry et al. 1995). Previous laboratory studies and field-scale artificial recharge experiments have demonstrated a time-dependent permeability reduction caused by trapped gases (Christiansen 1944; Bouwer 1966; Fayer and Hillel 1986; Constantz et al. 1988; Faybishenko 1995). Generally, the initial source of trapped gas is encapsulated air (mostly nitrogen and oxygen) and infiltration rates typically increase after this initial entrapped air has been displaced or dissolved by moving ground water (Christiansen 1944; Faybishenko 1995). Determining the percentage of porosity filled with trapped gas and subsequent changes in hydraulic conductivity is important in evaluating ponded and well-injected artificial recharge, permeable reactive barriers, in situ bioremediation, and ground water/surface water interaction beneath natural streams and lakes.

Gas-partitioning tracers can be used to distinguish between two fluid phases in porous media. The use of gas-partitioning tracers was developed initially by the petroleum industry to determine residual oil saturation in a two-fluid system with either water or gas (Tang and Harker 1991a, 1991b; Tang 1995). Retardation of gas-partitioning

[1]Corresponding author: U.S. Geological Survey, 2329 Orton Circle, Salt Lake City, UT 84119; (801) 908-5042; heilweil@usgs.gov

[2]Department of Geology and Geophysics, University of Utah, 135 S 1460 E, Salt Lake City, UT 84112; ksolomon@mines.utah.edu

[3]U.S. Geological Survey, Building 15, MS 421, 345 Middlefield Road, Menlo Park, CA 94025; kperkins@usgs.gov

[4]Formerly with U.S. Geological Survey, Placer Hall, 6000 J St., Sacramento, CA 95819. Now with Department of Civil and Environmental Engineering, The University of Melbourne, Parkville, Victoria 3010 Australia; ellettk@civenv.unimelb.edu.au

Received December 2002, accepted September 2003.

tracers has also been used at the field scale for determining the presence of dense nonaqueous phase liquids (Nelson and Brusseau 1996). Gas-partitioning tracers have been more recently applied for evaluating air-filled porosity in column and sand tank experiments (Fry et al. 1995; Fry et al. 1996; Donaldson et al. 1997; Vulava et al. 2002), and for evaluating water content in soil in a lysimeter (Nelson et al. 1999). Low-solubility dissolved gases will preferentially partition to the gas phase when they come into contact with trapped gas bubbles. Therefore, in hydrogeologic settings with trapped gas, the transport of low-solubility dissolved-gas tracers will be retarded when compared to nonpartitioning tracers, whose aqueous phase transport is not affected by the presence of gas. In both column and field experiments, Gupta et al. (1994) determined retardation factors in a shallow aquifer to be as high as 3.0 for dissolved helium, a low-solubility gas-partitioning tracer, as compared to chloride, a nonpartitioning tracer. This was attributed to the mass transfer of helium into small amounts of trapped gas.

The purpose of this study is to evaluate the amount of trapped gas in a porous medium under ponded conditions and its effect on vertical hydraulic conductivity and infiltration rates during artificial recharge. We believe that the study is the first of its kind to use a gas-partitioning tracer in a field-scale infiltration experiment for quantifying trapped gas.

Factors Affecting Infiltration Rates

Although some of the entrapped air in porous media beneath newly added surface water may migrate upward and escape to the atmosphere, much will remain trapped within the porous media until it dissolves into adjacent infiltrating water. This trapped gas will typically occur as bubbles in the largest pore spaces between the soil and rock grains, and will reduce the permeability of the material depending on its quantity, size, and uniformity of pore throats. Dissolution of this trapped gas should eventually occur because of an increase in hydrostatic pressure caused by the overlying ponded water. However, this process is very slow and is a function of the hydraulic head and the solubility of the individual gas. Because of its higher solubility, oxygen will be the first to dissolve, such that the composition of the remaining gas will primarily be nitrogen. If other processes such as siltation and biofilm development are minimal, the dissolution of trapped gas should cause an increase in infiltration rates.

Various temperature-dependent processes will affect surface water infiltration rates. Because the viscosity of water is temperature-dependent, hydraulic conductivity decreases as water temperature decreases. This effect could greatly reduce infiltration beneath shallow surface water bodies in areas with a large seasonal temperature decrease from summer to winter. A secondary temperature effect is the thermal contraction/expansion of trapped gas bubbles in the shallow subsurface caused by seasonal cooling/heating. This should have a smaller effect on infiltration rates than temperature-dependent variations in water viscosity. Finally, because of its retrograde solubility, trapped gas will dissolve at a higher rate in cooler water, enhancing the rate of permeability increase during winter months.

Long-term decreases in infiltration rates beneath ponded surface water basins have often been attributed to biological clogging and siltation. Traditionally, biological clogging has been described as a physical biofilm layer with lower hydraulic conductivity than that of the underlying porous media. However, recent studies (Beckwith and Baird 2001) indicate that long-term clogging may also be caused by the augmentation of entrapped air bubbles with biogenic gases such as methane, hydrogen, and carbon dioxide produced during bacterial respiration and decay (Donaldson et al. 1997; Beckwith and Baird 2001). The generation of gases such as methane, which has a low solubility, may partially, or completely, offset permeability increases associated with the dissolution of initially entrapped air. The rate of production of biogenic gases is likely higher in the summer months because of warmer water temperatures and increased photosynthesis.

Setting

A surface water reservoir was constructed in 2002 at Sand Hollow in southwestern Utah. It is expected that seepage beneath the reservoir will recharge the underlying Navajo Sandstone Aquifer. Water from the nearby Virgin River will be diverted to the reservoir during wetter periods for aquifer recharge; ground water will be withdrawn during drier periods to meet municipal needs. To evaluate potential recharge rates beneath Sand Hollow Reservoir, a 260-day infiltration pond experiment was conducted from July 2000 to May 2001 just north of the reservoir (Figure 1). The infiltration pond was circular with a radius of 30 m (Figure 2) and was constructed on undisturbed soils ~1 m thick (Figure 3). The soil at the infiltration pond site is silty sand, ranging in sand content from 50% to 80%. Beneath the soils is the Navajo Sandstone. It is better sorted than the overlying soils, with a typical grain size distribution of 90% sand. The sandstone is loosely cemented with calcite. Secondary near-vertical fractures are fairly evenly spaced at ~10 m increments at the site; the upper 3 m of these fractures are filled with calcrete. The uppermost meter of the Navajo Sandstone is weathered and capped with a thin (0.1 to 0.5 m) layer of calcrete. Depth to water beneath the infiltration pond prior to filling was ~20 m below land surface.

Methods

Field Methods

The 60 m diameter pond was filled initially on July 19, 2000. Water was provided throughout the experiment from a nearby production well. The water level within the pond was regulated by a float system and fluctuated by ~0.14 m between filling cycles. The average depth of the pond during the experiment was 0.46 m, resulting in an average pond volume of 980 m^3.

Thirty-two shallow piezometers were installed at the soil/sandstone contact in the 10 m wide berm surrounding the pond to evaluate the potential for lateral movement of water away from the pond. The majority of piezometers were located on the north side of the pond along a topographic depression in the bedrock contact. During the

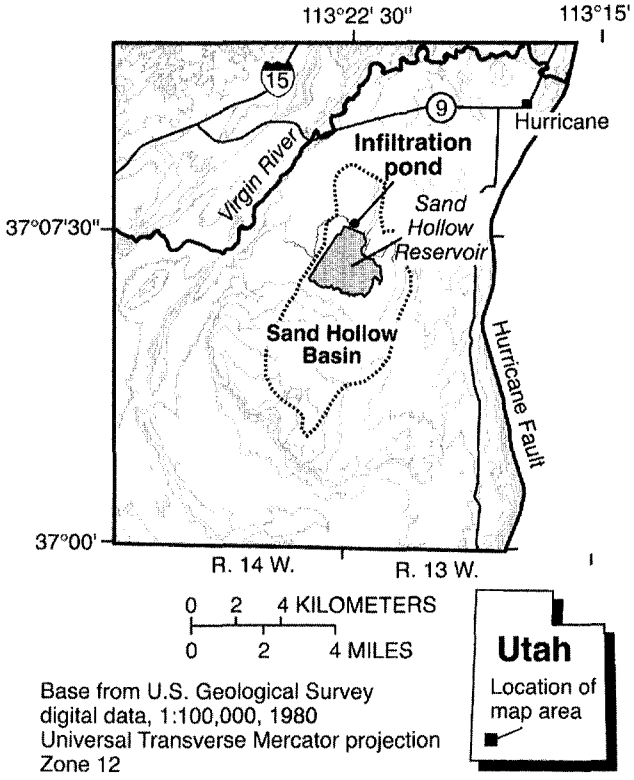

Figure 1. Location of the infiltration pond experiment site in Sand Hollow Basin, Utah.

experiment, ponded water was only observed in piezometers to a maximum distance of 3.5 m outward from the pond, indicating that lateral outflow was not occurring along the sandstone interface.

Seepage flux rates were calculated from metered volumetric flow into the pond and corrected for evaporation and precipitation. A 67 m pond diameter was used for this calculation because of the ponded conditions observed in piezometers at the bedrock contact up to a 3.5 m distance in the berm surrounding the pond. A 2.4 m diameter infiltration ring was also installed within the pond (Figure 2) and monitored throughout the experiment to compare point measurements of seepage flux rates to the average for the entire pond based on inflow.

To evaluate gas-filled porosity, dissolved helium gas and dissolved sodium bromide tracers were mixed into the pond on August 16, 2000, four weeks after the pond was initially filled. Bromide was selected as the nonpartitioning tracer because it is generally considered conservative due to its low sorption by anion exchange (Davis et al. 1980) and low background concentration in the water supply to the infiltration pond (< 0.2 mg/L). Helium-4 was selected as the gas-partitioning tracer because it is a nonreactive noble gas with a low natural concentration in shallow ground water (Carter et al. 1959). The background concentration of helium-4 in the water supply to the infiltration pond was about 4×10^{-8} cm^3/g of water at standard temperature and pressure (cm^3 STP/g water). Helium has a low solubility (6.75×10^{-3} cm^3 STP/g water) compared to other naturally occurring gases such as nitrogen (1.68×10^{-2} cm^3 STP/g water) and krypton (7.86×10^{-2} cm^3 STP/g water). Because helium is a naturally occurring nontoxic noble gas, health and safety concerns regarding its injection into a regional water supply aquifer were minimal.

Bromide was introduced to the pond by dissolving 420 kg of bromide (or 540 kg of sodium bromide, which is 77.65% bromide by weight) into a 1900 L tank of water, which was slowly mixed into 3.4×10^5 L of water that was added to the pond during a 4 hr period. Two sump pumps were used within the pond to mix the influent water containing bromide with the existing tracer-free pond water. The peak measured bromide concentration in the pond reached 430 mg/L. The steady decrease in bromide concentration was caused by the periodic inflow of tracer-free water to keep the pond full (Figure 4).

Dissolved helium was introduced to the pond during an 11.5 hr period beginning at the same time the bromide was added to the pond. This was accomplished by connecting welding-grade tank helium (99.995% pure) to eight MDB 600 ceramic-plate microbubblers (Point Four Systems, Richmond, British Columbia). These were deployed along the pond bottom and operated at ~200 kPa pressure, with an average flow rate of 3 L/min per microbubbler, creating bubbles between 100 and 500 μ in diameter. A total of 12 K size tanks of helium, totaling ~700 m^3 of helium gas under 1 atm pressure, were used for the tracer injection. The peak measured helium concentration in the pond was ~8.9×10^{-4} cm^3 STP/g water or ~10% of helium saturation, which is 8.22×10^{-3} cm^3 STP/g water at the 0.896 atm barometric pressure measured at the infiltration site. Helium concentration in the pond declined much more rapidly than bromide concentration because of exchange with the atmosphere (Figure 4).

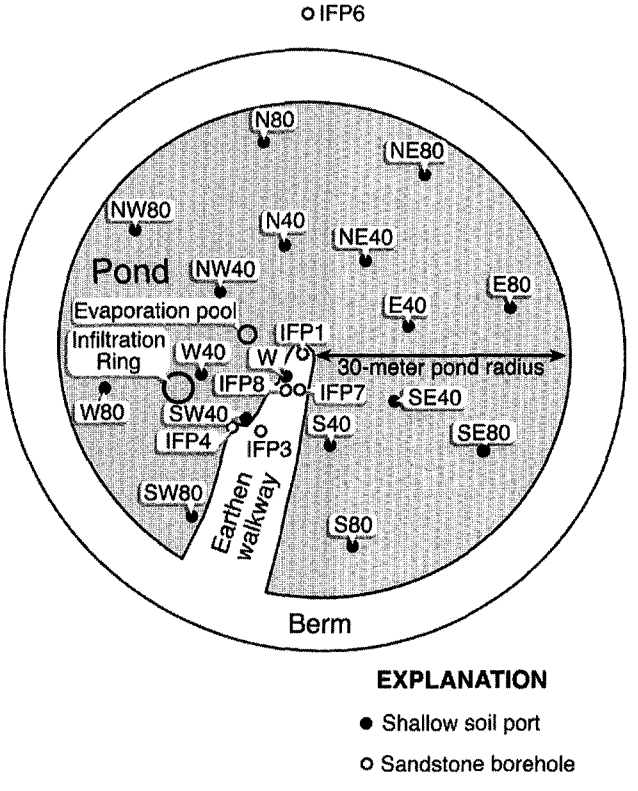

Figure 2. Sampling locations at the infiltration pond experiment site in Sand Hollow Basin.

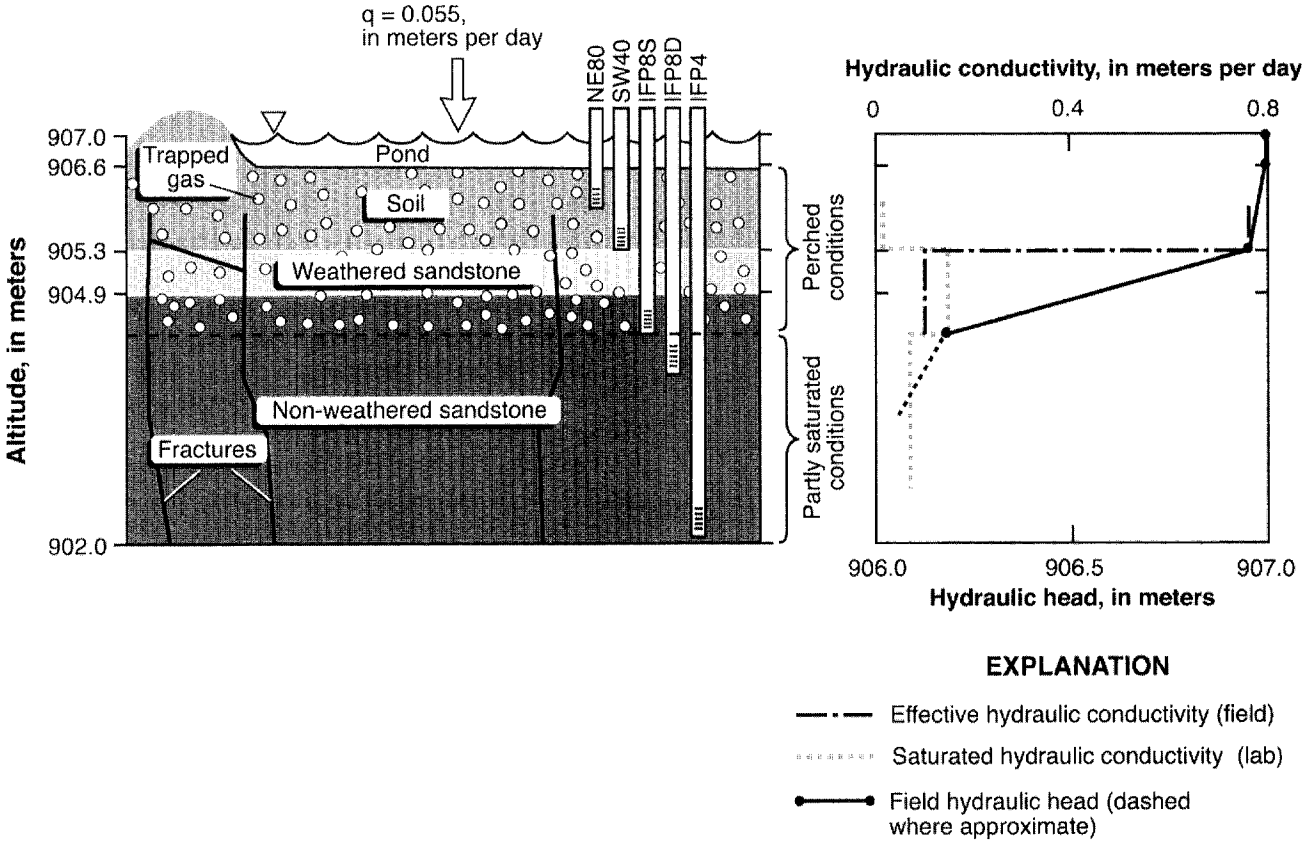

Figure 3. Schematic cross section of the infiltration pond showing generalized geology, hydraulic conductivity, and hydraulic-head measurements, Sand Hollow Basin.

Piezometers (2.2 cm diameter PVC) with 5 cm screen lengths were installed beneath the pond and used for collecting water samples and evaluating vertical hydraulic gradients down to 1.7 m depth in the soil and shallow sandstone, where ponded conditions existed. Bromide samples were collected and filtered into 125 mL polyethylene bottles by using 0.45 μ syringe-tip filters. Helium samples were collected with in situ diffusion samplers. The diffusion sampler method is described by Sheldon (2002) and consists of small 0.5 cm diameter by 5 cm long copper tubes with an internal headspace volume of ~0.3 cm^3 and gas-permeable silicon membranes. The diffusion samplers were installed at the depth of the perforated zone in each port and helium in the headspace allowed to equilibrate with the dissolved helium in the water for 24 hrs. These samples were quickly removed and cold-welded with a pinch-off tool.

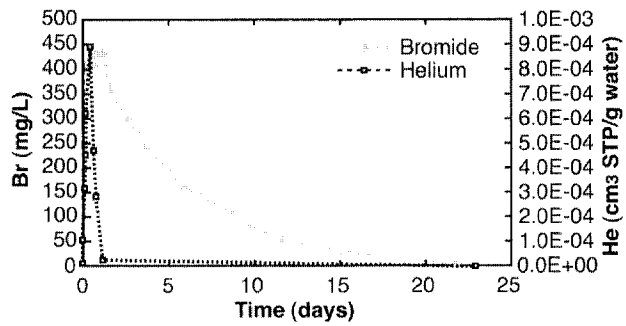

Figure 4. Measured bromide and helium concentration in pond water during the infiltration pond experiment at Sand Hollow Basin.

Model 1920 soil-water samplers (Soil Moisture Equipment Corp., Santa Barbara, California) were used for collecting water samples in the deeper unsaturated sandstone ports at the IFP3, IFP4, and IFP8 sites (Figure 2). These samplers were installed in 10 cm diameter open boreholes at depths of 2.4, 4.6, 7.6, 10.7, 14.0, and 16.7 m in the sandstone and backfilled with bentonite to prevent preferential flow. Vacuum pressure was applied to the soil-water samplers to induce the flow of water into a porous ceramic cup with a 500 mL collection chamber (Wood 1973). Pressurized air was then used to pump the sample into both polyethylene bottles for bromide analysis and 0.8 cm diameter copper tubes for helium analysis (Stute and Schlosser 2001). The collection method was lab-tested to ensure that degassing under vacuum would not affect helium concentrations.

Piezometers, tensiometers, and thermistors were used beneath the pond to evaluate hydraulic properties and temperatures during the infiltration pond experiment. Ports in the unconsolidated sand were installed with a hand auger; ports in the sandstone were installed in 10 cm diameter open boreholes in the sandstone. All the ports were backfilled with bentonite to prevent preferential flow. Water level measurements in 17 piezometers completed in soils and in one piezometer completed in shallow sandstone (IFP8S) were used to evaluate vertical hydraulic gradients between the pond and perched water to depths of 1.7 m beneath the pond. Deeper tensiometers and thermistors at the IFP3 and IFP4 sites were used to evaluate the water

potential (negative pressure head) and temperature at depths of 3, 6, 9, 12, 15, and 19 m in the underlying unsaturated sandstone between the pond and the regional water table.

Seepage flux rates were corrected for evaporation from the pond surface by using a 1 m diameter evaporation pool. In order to accurately represent water temperatures and wind conditions at the surface of the infiltration pond, the evaporation pool was located near the center of the pond (Figure 2). Water was added periodically to the pool and evaporation was determined by reading water level changes on a stage height gauge. Evaporation rates ranged from 0.001 to 0.01 m/day.

Laboratory Methods

Bromide samples from the pond and underlying ports were measured by the U.S. Geological Survey's National Water-Quality Laboratory with ion-chromatography methods with a detection limit of 0.05 mg/L. Helium concentrations were measured with both gas chromatography and mass spectrometry. Helium concentrations in the pond during the first 30 hrs were high enough to detect with a gas chromatograph. The method used for gas-chromatograph analysis of helium is described by Sugisaki and Taki (1987). It was necessary to use mass spectrometry to measure the low concentrations of helium ($< 1 \times 10^{-5}$ cm^3 STP/g water) at later times in the pond, as well as for all of the samples collected from the underlying ports. Replicate helium samples were collected and analyzed with both gas chromatograph and mass spectrometer methods. Replicate samples analyzed with the gas chromatograph were within 7% of each other. Replicates analyzed with the mass spectrometer were within 30%. Because the analytical precision for the mass spectrometer is < 1%, variation in replicates is attributed to either nonuniform sampling conditions or real variations at a given well between replicate samples. The observed variation in helium concentration throughout the duration of the test was several orders of magnitude and, thus, sampling/analytical errors are not significant.

Laboratory hydraulic properties of soil and sandstone core samples were determined for comparison to field observations and to provide a priori information on the permeability of the porous medium beneath the pond. The porosity of soil core samples was estimated by dividing the difference between particle and bulk densities by the particle density. The porosity of sandstone core samples was determined by dividing the difference between saturated and oven-dry mass by the sample volume. Measurements of saturated hydraulic conductivity were made on soil samples with the falling-head method (Reynolds et al. 2002) and on sandstone core samples with a flexible-wall permeameter (American Society for Testing and Materials 1998).

Measurements of variably saturated hydraulic conductivity were made on soil samples with the standard falling-head method (Klute and Dirksen 1986). The samples were saturated to varying degrees by using three different techniques. Because the first saturation technique was chosen to maximize trapped gas, no measures were taken to de-air the water prior to saturation. The air-dry core samples were set up for the falling-head experiment and allowed to saturate from the top. For the second technique, the samples were allowed to saturate from the bottom upward in a beaker of water, again with no de-airing of the water. For the third, the sample was placed in a beaker of de-aired water within a vacuum chamber at 635 mm mercury. The moisture content associated with each conductivity value was determined by weight at the end of the conductivity measurement. With these techniques, the samples reached saturations ranging from 68% to 98% of porosity. The three measurements serve to define the hydraulic conductivity relation, $K(\theta)$, at the wet end of the curve and therefore illustrate the effects of trapped gas on hydraulic conductivity.

Measurements of variably saturated hydraulic conductivity on sandstone samples were determined with the ultracentrifuge method for unsaturated hydraulic conductivity vs. saturation (Conca and Wright 1998). Measurements of matric potential vs. saturation were done on sandstone cores by using Tempe Cells and a pressure plate (Klute and Dirksen 1986).

Results

Laboratory Measurements of Hydraulic Properties

The porosity of 14 soil samples from in and around the pond had an arithmetic mean of 0.39 and a range of 0.29 to 0.45. Laboratory measurements of saturated hydraulic conductivity of these soil samples had a geometric mean of 0.02 m/day and a range of 0.004 to 0.06 m/day. The porosity of four shallow weathered sandstone core samples from a depth of ~1 m had an arithmetic mean of 0.22 and a range of 0.20 to 0.26. The geometric mean saturated hydraulic conductivity value of these samples was 0.17 m/day and ranged from 0.10 to 0.23 m/day. The porosity of 13 deeper nonweathered sandstone core samples (2 to 19 m depth) had a geometric mean of 0.24 and a range of 0.20 to 0.27. The geometric mean saturated hydraulic conductivity value of these samples was 0.10 m/day and ranged from 0.01 to 0.42 m/day.

Although the saturated hydraulic conductivity of the soil samples is lower than that of the sandstone, laboratory tests on partially saturated core samples indicate that an air-filled porosity of only a few percent reduces the effective hydraulic conductivity of the sandstone to lower values than that of the soil. The hydraulic conductivity value of a sandstone core from the IFP7 site decreased by an order of magnitude from 0.17 to 0.017 m/day as saturation was decreased by 10% (Figure 5). In contrast, the hydraulic conductivity value of a soil sample from the NE80 site decreased by only ~10% from 0.052 to 0.048 m/day as saturation was decreased by > 30%. Measurements on a soil sample from the NE40 site yielded similar results (not shown). Therefore, the sandstone sample has a higher fully saturated, yet lower partially saturated, hydraulic conductivity value than the soil.

Field Hydraulic Measurements

Seepage flux rates from the infiltration pond, determined from metered volumetric flow into the pond and corrected for both evaporation and precipitation, rapidly decreased from > 0.15 m/day of water during the initial wetting-up period to an average of 0.05 m/day from August

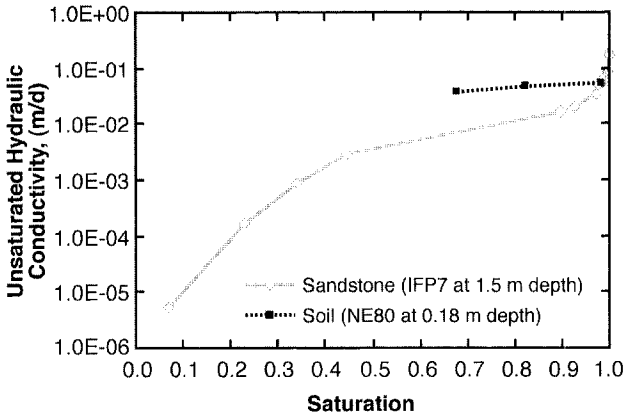

Figure 5. Variably saturated hydraulic conductivity values of sandstone and soil samples at the infiltration pond in Sand Hollow Basin.

to February (Figure 6). Average seepage flux rates increased slightly to 0.06 m/day during February and March, and then remained steady until the end of the experiment in early May. Except for the initial 8-day wetting-up period, the average seepage flux rate throughout the 10-month experiment was 0.055 m/day. This is very similar to seepage flux measurements from the 2.4 m diameter infiltration ring, which averaged 0.047 m/day for the same time interval. Assuming a mean porosity of 0.39 for the shallow soils, the average linear velocity through the soils beneath the pond was ~0.14 m/day from August to May.

The average matric potentials from tensiometers installed at 3.0, 5.9, and 8.7 m depths at the IFP3 site (Figure 2) during the tracer experiment were +0.036 ± 0.019, – 0.046 ± 0.008, and – 0.053 ± 0.007 bars, respectively (+37 ± 19, – 47 ± 8, and – 47 ± 7 cm of water). This implies that there was a transition from saturated to unsaturated conditions beneath the pond between depths of 3.0 to 5.9 m at this site. Similarly, at the IFP8 site, nested ports showed standing water at a depth of 1.7 m, yet dry conditions in a piezometer at a depth of 6.1 m. Unsaturated moisture-retention data from a sandstone core sample collected from beneath the pond indicate that at matric potentials of ~–0.05 bars, the sandstone would be ~75% saturated (25% gas-filled).

Vertical hydraulic gradients were measured between the pond and 17 ports in both the shallow soils and in the weathered sandstone three separate times during February 2001. The average vertical gradient for the shallow soil ports ranged from 0.01 to 0.24, with a geometric mean of 0.08. The average standard deviation of the replicate measurements was 0.01. This large range in vertical gradients within the soils implies the occurrence of preferential flow, possibly caused by a combination of variable amounts of trapped gas and heterogeneous porous media. The average seepage flux rate from the infiltration pond during the time of the vertical gradient measurements was 0.055 m/day (Figure 6). Field-based vertical hydraulic conductivity values, calculated using Darcy's law, are estimated to range from 0.2 to 6.8 m/day for the shallow soils. An average vertical gradient of 0.39 was measured between the pond and the IFP8S port, finished in the underlying weathered sandstone. The vertical hydraulic conductivity value of the weathered sandstone, also using Darcy's law, was 0.13 m/day. Therefore, although the weathered sandstone has a higher laboratory-determined saturated hydraulic conductivity value than does the soil, the larger observed vertical gradient produces an effective field hydraulic conductivity value of the weathered sandstone that is lower than that of the soil (Figure 3). This is consistent with the lower laboratory unsaturated hydraulic conductivity values of sandstone compared to the soil (Figure 5). In addition, laboratory saturated vertical hydraulic conductivity values were much lower (0.004 to 0.06 m/day) than estimated field hydraulic conductivity values (0.2 to 6.8 m/day) at the 12 shallow soil ports beneath the pond. This difference is likely caused by field-scale preferential flow pathways not represented in the small diameter (5 cm) core samples used in the laboratory measurements.

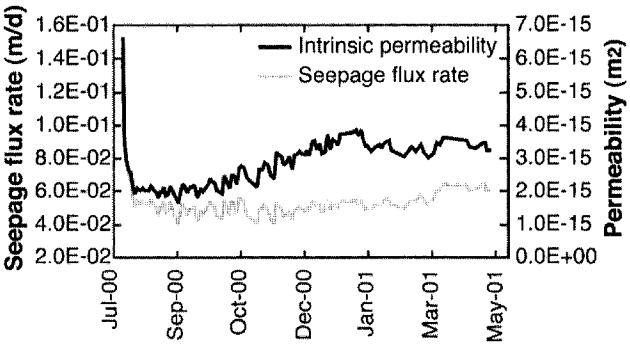

Figure 6. Seepage flux rate and estimated intrinsic permeability of soils during the infiltration pond experiment at Sand Hollow Basin.

Tracer Concentrations and Breakthrough Curves

Peak helium concentration at five ports occurred between 21 and a minimum of 258 days after the bromide tracer peak. The ratio of helium to bromide arrival times indicates that the helium peak was retarded by factors ranging from 2 to > 11 (Table 1). A typical breakthrough curve for both bromide and helium is shown in Figure 7. In general, the observed helium breakthrough displayed the following three characteristics: (1) great attenuation and retardation of helium compared to bromide, (2) an early first arrival of helium before the main helium breakthrough curve, and (3) increased loss of helium mass with depth.

Interpretation and Modeling

The CXTFIT code (Toride et al. 1999) for simulating one-dimensional solute transport was used to model bromide and helium breakthrough curves at the five ports beneath the pond.

Bromide Transport

Bromide transport was considered conservative (no adsorption, decay). The one-dimensional advection-dispersion equation used to simulate bromide transport (modified from Toride et al. [1999]) is

$$\frac{\partial c}{\partial t} = D\frac{\partial^2 c}{\partial x^2} - v\frac{\partial c}{\partial x} \qquad (1)$$

Table 1
Arrival Times of Peak Bromide and Helium Concentration at Various Ports Beneath the Infiltration Pond at Sand Hollow Basin, Utah

Port	Depth (m)	Geologic Media	Bromide Peak (mg/L)	Date	Elapsed Days	Helium Peak (cm^3 STP/g water)	Date	Elapsed Days	Observed Retardation
NE80	0.76	soil	211	9/4/00	19	1.21E-06	12/19/00	125	6.6
SW40[1]	1.25	soil	196	9/6/00	21	1.94E-06	9/27/00	42	2
IFP8S	1.68	weathered sandstone	72	9/27/00	22	1.08E-06	2/16/01	184	8.4
IFP8D[2]	2.44	sandstone	66	9/7/00	22	1.68E-07	4/30/00	258	> 11.7
IFP4	4.58	sandstone	135	9/7/00	22	2.81E-07	2/16/01	184	8.4

[1]Observed helium and bromide at the SW40 port both showed double peaks. Although helium concentration was nearly identical for both peaks, the second peak was chosen because bromide concentrations were much higher in the second peak.
[2]Calculations for the IFP8D port assume the helium peak of the breakthrough curve occurred at the end of the infiltration pond experiment. Actual peak may have occured later if test was continued, resulting in a larger observed helium retardation.

where c = the dissolved bromide concentration in water (mg/L), t = time (day), D = dispersion coefficient (m^2/day), x = distance (m), and v = average pore water velocity (m/day).

It was not possible to accurately represent bromide concentrations at various ports with uniform values of dispersivity and average linear velocity, indicating the heterogeneous nature of the system. Rather, values of dispersivity and velocity were determined for each of the five ports by curve fitting of simulated breakthrough curves to the observed bromide concentrations. A typical match between observed and simulated bromide breakthrough is shown in Figure 8. Consistent with findings from other studies (Domenico and Schwartz 1998), dispersivity values generally increased with flowpath distance, ranging from 0.02 m for two shallow ports to 0.50 m for the deepest port (Table 2). Average simulated pore water velocity for the shallowest four ports ranged from 0.05 to 0.08 m/day. The velocities for the two soil ports (~0.05 to 0.06 m/day) are somewhat less than the average linear velocity of 0.14 m/day estimated for the soils based on the average seepage flux rate of 0.055 m/day. Differences between the average pore water velocity beneath the pond and simulated velocities at specific locations based on bromide breakthrough curves are likely caused by heterogeneities in the soils and sandstone. The deepest port (IFP4), completed in the sandstone, had a much higher average pore water velocity (0.22 m/day) than the shallower ports. This likely is caused by preferential flow associated with fractures in the sandstone. When this borehole was initially drilled, air was observed to blow out of a nearby borehole, indicating the presence of a connected fracture between the two wells.

Helium Transport

Average linear velocity and dispersivity values determined from the bromide breakthrough curve for each port were used for fitting the observed helium breakthrough curves. The observed retardation of helium transport relative to average pore water velocity indicates the presence of a gas phase beneath the infiltration pond. Assuming sorption of helium on solids is negligible (Nelson and Brusseau 1996) and helium equilibrium between gas and liquid phase as defined by Henry's law, the retardation factor, R, can be used to estimate gas-filled porosity from

$$R = 1 + H' \frac{V_g}{V_w} \tag{2}$$

where V_g/V_w is the volumetric gas-to-water ratio and H' is the dimensionless Henry's law constant (Fry et al. 1995). This simple one-region equilibrium model was tested but could not reproduce the observed helium breakthrough (represented in Figure 9 as R = 10). As previously reported

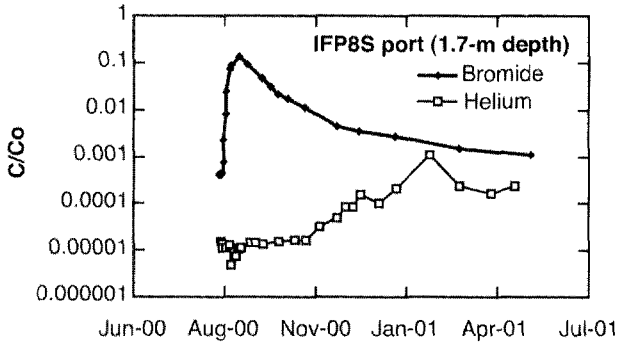

Figure 7. Observed bromide and helium breakthrough at the IFP8S port during the infiltration pond experiment at Sand Hollow Basin.

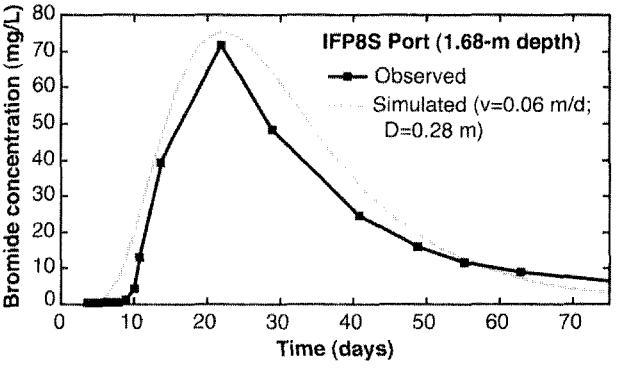

Figure 8. Observed and simulated bromide breakthrough at the IFP8S port during the infiltration pond experiment at Sand Hollow Basin.

Table 2

Transport Properties and Gas-Filled Porosity Values Calculated from Observed and Simulated Bromide and Helium Concentrations During the Infiltration Pond Experiment at Sand Hollow Basin, Utah

Port	Depth (m)	Observed Retardation	Average Pore-Water Velocity (m/day)	Dispersivity (m)	First-Order Mass Transfer Coefficient, α (d^{-1})	First-Order Decay Constant, μL (d^{-1})	Simulated Retardation[1]	Average Port Temperature (°C)	Dimensionless Henry's Law Constant, H'	Volumetric Gas-to-Water V_g/V_w	Percent of Gas-Filled Porosity, V_g
NE80	0.76	6.6	0.05	0.02	0.03	0.05	14	16	96.2	0.135	0.12
SW40	1.25	2	0.06	0.02	0.03	0.04	8	16	96.2	0.073	0.07
IFP8S	1.68	8.4	0.06	0.28	0.11	0.06	15	16	96.2	0.146	0.13
IFP8D[2]	2.44	> 11.7	0.08	0.38	0.02	0.07	> 35	15.1	96.5	0.352	0.26
IFP4	4.58	8.4	0.22	0.50	0.06	0.13	14	15.4	96.4	0.135	0.12

[1]Simulated helium breakthrough curves use the nonequilibrium (kinetic) advection/dispersion equation with first order decay.
[2]Calculations for thr IFP8D port assume helium peak of the breakthrough curve occurred at the end of the infiltration pond experiment. The actual peak may have occured later if the infiltration pond experiment were continued. Therefore, the simulated retardation, volumetric gas-to-water ratio, and gas-filled porosity reported in this table are minimum values.

by Donaldson et al. (1997) and Vulava et al. (2002), dissolved-gas tracer concentrations may not be in equilibrium with concentrations in the gas phase. Rather, the exchange of helium between aqueous and gaseous phases may be kinetically limited, depending on both the ratio of surface area to volume of the aqueous and gaseous phases, and the transport velocity. To simulate these kinetic effects, helium breakthrough was simulated by using a dimensionless form of the two-region (mobile, immobile) nonequilibrium transport equation (modified from Toride et al. [1993]):

$$\beta R\frac{\partial C}{\partial t} = \frac{1}{P}\frac{\partial^2 C}{\partial Z^2} - \frac{\partial C}{\partial Z} - \omega[C - C_{im}] \qquad (3)$$

where β is the partitioning coefficient, and C (dimensionless concentration of the mobile fraction), P (Peclet number), Z (dimensionless length), T (dimensionless time), ω (dimensionless mass transfer coefficient), and C_{im} (dimensionless concentration of the immobile fraction) are defined as

$$C = \frac{c}{c_o} \qquad P = \frac{vL}{D} \qquad Z = \frac{x}{L}$$

$$T = \frac{vt}{L} \qquad \omega = \frac{\alpha(R-1)L}{v} \qquad C_{im} = \frac{c_{im}}{c_{o_{im}}}$$

with L being the characteristic length (m) representing the depth of the port beneath the infiltration pond, and α is the first-order kinetic rate coefficient (d^{-1}) controlling helium mass transfer between aqueous and gaseous phases. Larger mass-transfer coefficients indicate more limited interaction between these phases. Initially, a uniform simulated mass-transfer coefficient was used for all of the ports, but this did not produce satisfactory results. This indicates that fluid velocities and geometries of trapped gas bubbles were not uniform at the various ports. Rather, simulated values for the mass-transfer coefficient, α, ranged from 0.02 to 0.11 d^{-1} (Table 2).

This kinetically limited interaction produced simulated helium breakthrough curves (represented in Figure 9 as R = 20, α = 0.03/day) that were much closer to observed values than did the equilibrium advection/dispersion/retardation equation. However, later-time simulated helium values were still higher than observed values. This implies that a mass loss of helium occurred between the pond and the ports. This observation is significantly different from previously reported gas-partitioning column tracer experiments and illustrates the complexities associated with applying a laboratory-verified method in a field setting.

Two possible causes for this are helium loss through upward air bubble migration from beneath the pond and diffusional helium loss laterally away from the soils beneath the infiltration pond through a connected gas phase. Although pervasive upward air bubbling through the pond was observed during the first few days after it was initially filled, this was not observed during the helium/bromide tracer test,

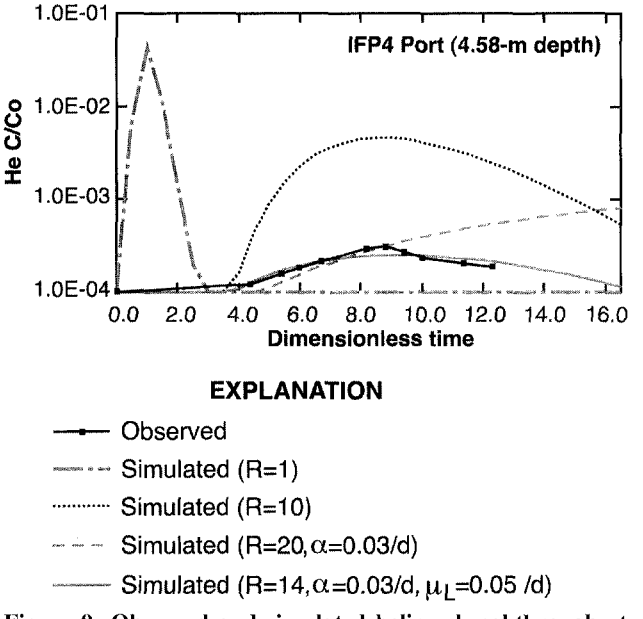

Figure 9. Observed and simulated helium breakthrough at the IFP4 port during the infiltration pond experiment at Sand Hollow Basin.

so it was assumed not to be significant. Calculations of diffusional loss were made assuming that 10% of the average 40% porosity of the pond soils was gas-filled. An analytical solution to the diffusion equation was applied by representing the pond as a solid 30 m radius cylinder with uniform initial helium concentration and an outside boundary condition of zero helium concentration (Crank 1975). This calculation indicates that > 40% of the initial helium mass may have been lost by lateral gaseous diffusion during the 260-day experiment. Because the presence of water in the shallow ports indicated saturated conditions, regions of both connected gas and liquid phases may have existed in the same porous media. This may be caused by dual permeability, particularly for multiphase (unsaturated) flow in the sandstone, where the flow of gas may occur through larger connected pore spaces such as fractures and the flow of the water may occur through the matrix (Pruess 2002).

Therefore, a first-order decay term was used with the nonequilibrium advection/dispersion equation (Toride et al. 1993) to simulate diffusive loss of helium laterally away from the pond:

$$\beta R\frac{\partial C}{\partial t} = \frac{1}{P}\frac{\partial^2 C}{\partial Z^2} - \frac{\partial C}{\partial Z} - \omega[C - C_{im}] - \mu_1 C \quad (4)$$

where μ_1 is a dimensionless first-order decay coefficient, defined as $\mu_1 = \frac{L\mu_L}{v}$ with μ_L (d^{-1}) being the first-order decay coefficient for the aqueous phase (dissolved) helium.

A uniform decay constant was initially used for all of the ports, but produced an unsatisfactory match between measured and simulated helium concentrations. Rather, decay constants varying from 0.04 to 0.13/day were used, resulting in substantially improved fits between observed and simulated helium breakthrough (represented in Figure 9 as R = 14, α = 0.03/day, μ_L = 0.05/day), especially with respect to the tail at later time (Figures 9 and 10). One interesting characteristic of both the observed and simulated helium breakthrough in the two shallow soil ports (NE80 and SW40) is an early small peak prior to the main helium peak. Simulated retardation factors determined by using this kinetically limited advection/dispersion equation with first-order decay ranged from 8 to > 35. The volumetric gas-to-water ratio (V_g/V_w) of the porous media at the five ports beneath the pond was calculated by using these retardation factors in Equation 2 (Table 2). The dimensionless Henry's law constant (H′) used in the equation varied from port to port, depending on the average water temperature during the experiment. The percent of porosity filled with gas (V_g) was then calculated by using the relation

$$V_g = \frac{1}{1 + \frac{V_w}{V_g}} \quad (5)$$

These calculations indicate that 7% to 26% of the porosity in the first few meters beneath the pond was gas-filled.

The simulated first-order decay constant, μ_L, used to represent the loss of helium mass with depth, increased with flowpath distance. Values ranged from ~0.05 for the shallowest three ports (depths of 0.76 to 1.68 m) to 0.13 for the deeper port at a 4.57 m depth (Table 2). This is consistent with observations of increasingly unsaturated conditions with depth beneath the pond. Such an increasingly connected gas phase with depth would result in a larger loss of helium tracer mass with depth.

Discussion

Water level and matric potential measurements from piezometers and tensiometers beneath the pond during the infiltration pond experiment indicated saturated conditions (and thus disconnected trapped gas bubbles) down to depths of 2 to 3 m. However, the 7% to 13% gas-filled porosity calculated for the three shallow ports (Table 2) is based on the assumption that some of the helium tracer was lost laterally outward along connected air pathways in the soil and sandstone, such as fractures and root casts. These pathways may not have been completely saturated, especially during early time transient conditions, when the larger pore throats would saturate later than the finer grained matrix. The occurrence of coexisting saturated matrix conditions and a connected gas phase in fractures has previously been suggested (Pruess 2002) and may indicate that abrupt lateral transitions between fully and partially saturated conditions occurred across short distances in heterogeneous media.

At depths > 2 m beneath the bottom of the pond, negative matric potential measurements at tensiometers indicated partially saturated conditions. This is consistent with the larger range in estimated gas-filled porosity at the two deeper ports of 12% to 26%. The 12% gas-filled porosity at the IFP4 port (4.6 m deep) likely represents a connected gas phase, based on the need to apply a vacuum to retrieve water from the soil-water sampler at that depth. In addition, tensiometer measurements both 1.5 m above and 1.5 m below the IFP4 port show that the port was in the transition zone between shallow saturation and deeper, partially saturated conditions. However, the high pore water velocity at the port and the similar gas-filled porosity values (7% to 13%) at shallower saturated ports indicate that the matrix at IFP4 was nearly saturated. The larger amount of gas-filled porosity (26%) at the IFP8D port (2.4 m deep) clearly represents partially saturated conditions; a vacuum was also needed at this port to retrieve water from the soil-water sampler. The lesser degree of saturation at this port compared to IFP4 may have been caused by a moisture-shadow effect, as this port was located beneath the center of a 5 m wide earthen walkway that extended out into the pond (Figure 2).

Air initially trapped in porous media beneath artificial recharge basins will eventually dissolve into the infiltration water passing through because of the increased solubility of gas with increasing hydrostatic pressure. An increase in hydrostatic pressure of 1.5 m of water (the midpoint of the ~3 m thick column of water and saturated porous medium at the infiltration pond) will increase nitrogen solubility by 0.0025 cm^3 (STP)/g water. Assuming a 2 m thick layer of

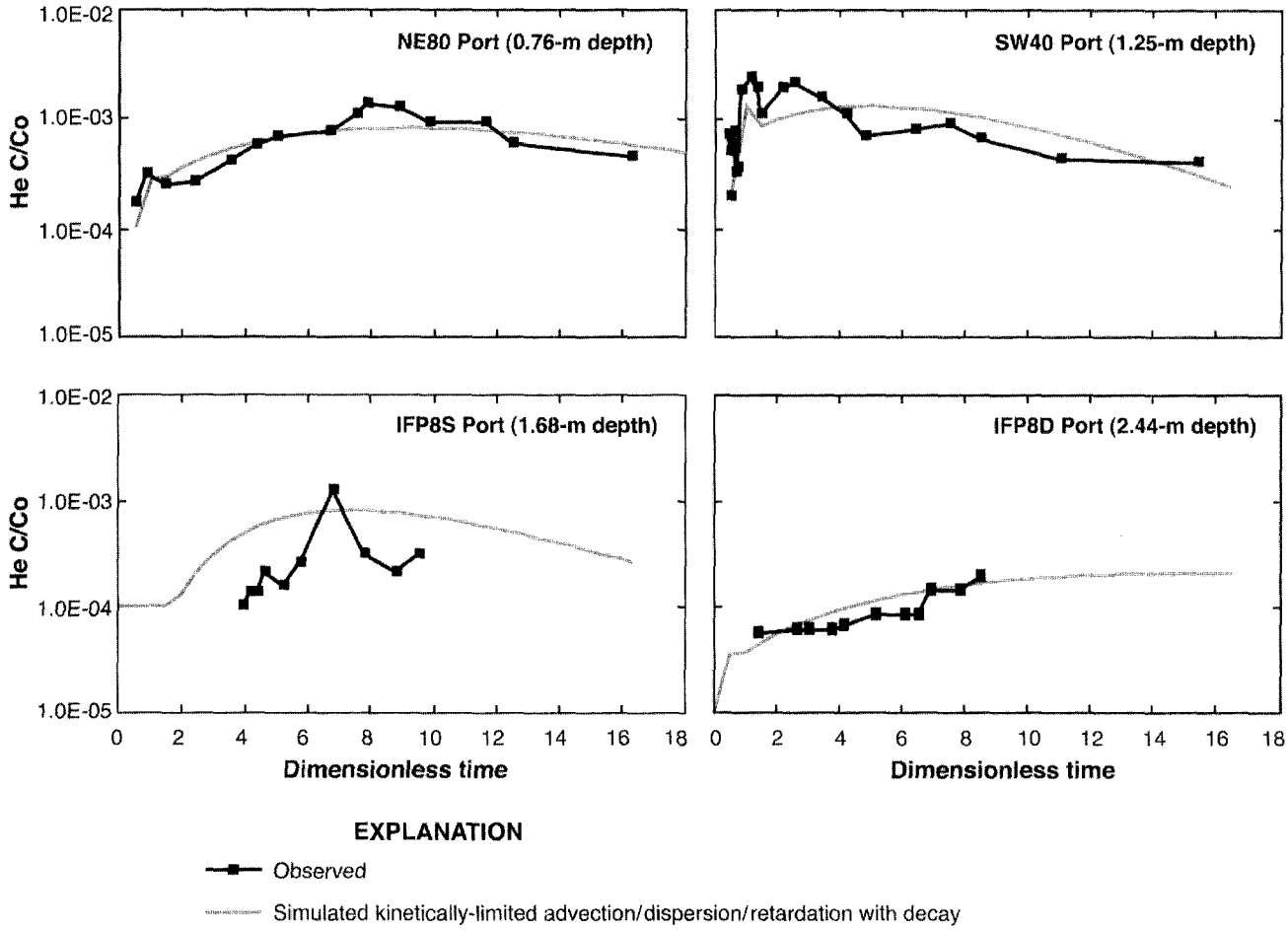

Figure 10. Observed and simulated helium breakthrough at various ports during the infiltration pond experiment at Sand Hollow Basin.

soil and sandstone beneath the infiltration pond (surface area of 2000 m^2) with an average porosity of 30%, the volume of saturated pore space beneath the pond during the experiment was ~1200 m^3. If 10% of this porosity was initially air-filled (mostly nitrogen), the initial volume of trapped gas would have been ~120 m^3. Assuming an average seepage flux rate of 0.055 m/day (a volumetric flux rate of ~100 m^3/day), it would take ~500 days (1.4 years) for the trapped gas to completely dissolve. Dissolution of this trapped gas would cause increased permeability over time.

Much of the variation in infiltration rates during the experiment is attributed to changes in water viscosity associated with varying water temperatures (5°C in the winter to 30°C in the summer) measured in the shallow soil ports beneath the pond. This results in a dynamic viscosity range of 0.008 to 0.015 g/cm per sec. In order to evaluate only the changes in the trapped gas, the intrinsic permeability of the soil beneath the pond was calculated by using Darcy's law. After the initial wetting period in July, the intrinsic permeability of the material beneath the pond generally rose from ~2×10^{-15} m^2 in August to almost 4×10^{-15} m^2 in December (Figure 6). Permeability was fairly constant from December to May, averaging ~3.4×10^{-15} m^2. The data indicate that the increase in permeability from August to December was caused primarily by the dissolution of the initial entrapped air, along with some thermal contraction of the overall volume of this air. Assuming an initial entrapped air volume of 120 m^3, the decrease in temperature of the shallow soils from 30°C in July to 5°C in January would reduce this volume by ~ 8% to 110 m^3. In addition, because of its retrograde solubility, the solubility of a gas bubble containing 100% nitrogen would increase from 0.0091 cm^3 (STP)/g water at 30°C to 0.0148 cm^3 (STP)/g water at 5°C. The more constant permeability values from December to May indicate that increase in permeability caused by continued dissolution of the initially entrapped air was offset by a combination of (1) thermal expansion of the trapped gas; (2) increased biogenic gas-production rates, as evidenced by higher concentrations of dissolved methane, carbon dioxide, and hydrogen in water samples beneath the pond; and (3) increased clogging caused by a biofilm/silt layer that gradually developed beneath the pond during the experiment. Time-dependent permeability variations caused by changing volumes of trapped gas in otherwise saturated porous media introduce an additional complexity to numerical modeling of infiltration. Models of fluid flow through variably saturated porous media typically use the Richards' equation by applying fitting parameters to laboratory tests of matric potential or hydraulic conductivity vs. saturation and do not account for transient permeability variations caused by trapped gas. In order to account for changing permeability of the porous media, the values defined in the model for saturated hydraulic conductivity would have to include

temporal variations in trapped gas content. In addition, under nonisothermal conditions, either intrinsic permeability would have to be explicitly defined or transient changes in saturated hydraulic conductivity resulting from temperature-varying fluid viscosity and thermal contraction/expansion of trapped gas bubbles would have to be input to the model.

Summary and Conclusions

The observed retardation of helium relative to bromide during an infiltration pond tracer experiment indicated the presence of substantial amounts of gas-filled porosity beneath the pond. Simulations of helium breakthrough by using both (1) equilibrium advection/dispersion with retardation and (2) kinetically limited advection/dispersion/retardation with kinetic mass transfer between the trapped gas and water were not able to closely approximate observed helium concentrations. However, breakthrough curves were reasonably simulated by including a decay term to represent the diffusive loss of helium through interconnected gas-filled pore spaces. This finding is significant in that it illustrates a difficulty in applying the laboratory-verified gas-partitioning tracer method to a field-scale experiment. Because saturated conditions were measured with piezometers and tensiometers to a depth of at least 2 m, the observed mass loss of helium indicates regions of both connected gas and fluid phases in the same porous media, particularly during early time when the smaller pore throat diameters of the matrix would saturate before larger-diameter preferential pathways. Simulations done with both a first-order decay term to represent helium mass loss and a kinetic helium mass transfer coefficient between liquid and gas resulted in simulated retardation factors ranging from 8 to 15 at three shallow ports. This, along with water level measurements in shallow piezometers, indicates that ~7% to 13% of the porosity in the first 2 m beneath the bottom of the pond contained trapped gas under saturated conditions. Two ports at depths > 2 m had simulated retardation factors of 14 to 35, indicating that ~12% to 26% of the pore space was filled with gas under partially saturated conditions. This is consistent with piezometer, tensiometer, and soil-water sampler measurements deeper than ~2 m beneath the pond.

The trapped gas beneath the infiltration pond would exist mostly in the larger pore throats. While laboratory tests indicate that the saturated hydraulic conductivity in the shallow soils is ~10 times lower than in the underlying weathered sandstone, the effective hydraulic conductivity of the sandstone with 10% air-filled porosity is much lower than that of the sand. This may be caused by the more uniform pore throat diameters of the well-sorted sandstone. The lower effective hydraulic conductivity of the sandstone is consistent with in situ hydraulic-gradient measurements made during the experiment, which indicated steeper hydraulic gradients between the pond and the sandstone than between the pond and the shallow soils.

Infiltration rates at other artificial recharge basins underlain by well-sorted materials may also be limited by trapped gas. One common management practice is to periodically dry out artificial recharge basins and physically break up silt and biofilm layers. However, this dry tilling will reintroduce trapped gas, partly offsetting permeability gains. Instead, wet tilling is an alternative for breaking up the silt/biofilm layer without reintroducing trapped gas. Such a technique may be more effective for optimizing the permeability of recharge basins, especially those underlain by well-sorted porous medium with fairly uniform pore throat diameters.

Trapped gas under naturally occurring conditions may also limit infiltration and recharge. Similar to artificial recharge, surface ponding of water during ephemeral flooding events in washes and playa basins will entrap air in the underlying porous media and reduce its effective permeability. The duration of such events generally ranges from hours to months. The relatively slow dissolution of entrapped air indicates that effective infiltration rates during these natural events may be much less than estimates based on laboratory permeability analyses.

Acknowledgments

We thank Ronald Thompson of the Washington County Water Conservancy District and Dennis Watt of the Bureau of Reclamation for their financial support of this research, Alan Rigby of the University of Utah Dissolved Gas Service Center for assistance with mass spectrometer analysis of dissolved-gas samples, Joel Hubbell and James B. Sisson of the Idaho National Engineering and Environmental Laboratory for assistance with installing tensiometers beneath the infiltration pond, and Peter Kroopnick and two anonymous reviewers for their thorough and thoughtful reviews of the manuscript. James Constantz, Alan Flint, and John Nimmo of the U.S. Geological Survey (USGS) also provided very helpful internal USGS reviews. Publication is authorized by the director of the USGS.

Author's Note: The use of brand names in peer-reviewed papers is for identification purposes only and does not constitute endorsement by the USGS.

Editor's Note: The use of brand names in peer-reviewed papers is for identification purposes only and does constitute endorsement by the authors, their employers, or the National Ground Water Association.

References

American Society for Testing and Materials. 1998. Standard test method for measurement of hydraulic conductivity of saturated porous materials using a flexible wall permeameter, D 5084 (1990). In *1998 Annual Book of ASTM Standards*, vol. 04.09, 62–69. West Conshohocken, Pennsylvania: American Society for Testing and Materials.

Beckwith, C.W., and A.J. Baird. 2001. Effect of biogenic gas bubbles on water flow through poorly decomposed blanket peat. *Water Resources Research* 37, no. 3: 551–558.

Bouwer, H. 1966. Rapid field measurement of air entry value and hydraulic conductivity of soil as significant parameters in flow system analysis. *Water Resources Research* 2, no. 4: 729–738.

Carter, R.C., W.J. Kaufman, G.T. Orlob, and D.K. Todd. 1959. Helium as a ground-water tracer. *Journal of Geophysical Research* 64, no. 12: 2433–2439.

Christiansen, J.E. 1944. Effect of entrapped air upon the permeability of soils. *Soil Science* 58, no. 5: 355–365.

Conca, J.L., and J. Wright. 1998. The UFA method for rapid, direct measurements of unsaturated transport properties in soil, sediment, and rock. *Australian Journal of Soil Research* 36, no. 2: 291–315.

Constantz, J., W.N. Herkelrath, and F. Murphy. 1988. Air encapsulation during infiltration. *Soil Science Society of America Journal* 52, 10–16.

Crank, J. 1975. *The Mathematics of Diffusion*. London: Oxford University Press.

Davis, S.N., G.M. Thompson, H.W. Bentley, and G. Stiles. 1980. Ground-water tracers—A short review. *Ground Water* 18, no. 1: 14–23.

Domenico, P.A., and F.W. Schwartz. 1998. *Physical and Chemical Hydrogeology*. New York: John Wiley and Sons.

Donaldson, J.H., J.D. Istock, M.D. Humphrey, K.T. O'Reilly, C.A. Hawelka, and D.H. Mohr. 1997. Development and testing of a kinetic model for oxygen transport in porous media in the presence of trapped gas. *Ground Water* 35, no. 2: 270–279.

Faybishenko, B.A.1995. Hydraulic behavoir of quasi-saturated soils in the presence of entrapped air: Laboratory experiments. *Water Resources Research* 31, no. 10: 2421–2435.

Fayer, M.J., and D. Hillel. 1986. Air encapsulation, 1. Measurement in a field soil. *Soil Science Society of America Journal* 50, 586–572.

Fry, V.A., J.D. Istok, L. Semprini, K.T. O'Reilly, and T.E. Buscheck. 1995. Retardation of dissolved oxygen due to a trapped gas phase in porous media. *Ground Water* 33, no. 3: 391–398.

Fry, V.A., J.D. Istok, and K.T. O'Reilly. 1996. Effect of trapped gas on dissolved oxygen transport—Implications for in situ bioremediation. *Ground Water* 34, no. 2: 200–210.

Gupta, S.K., L.S. Lau, and P.S. Moravcik. 1994. Ground water tracing with injected helium. *Ground Water* 32, no. 1: 96–102.

Klute, A., and C. Dirksen. 1986. Hydraulic conductivity and diffusivity: Laboratory methods. In *Methods of Soil Analysis, Part 1: Physical and Mineralogical Methods*, 2nd edition, ed. A. Klute. Madison, Wisconsin: American Society of Agronomy, Soil Science Society of America.

Nelson, N.T., and M.L. Brusseau. 1996. Field study of the partitioning tracer method for detection of dense nonaqueous phase liquid in a trichloroethene-contaminated aquifer. *Environmental Science & Technology* 30, no. 9: 2859–2863.

Nelson, N.T., M.L. Brusseau, and T.D. Carlson. 1999. A gas-phase partitioning tracer method for the in situ measurement of soil water content. *Water Resources Research* 35, no. 12: 3699–3707.

Pruess, K.C. 2002. Modeling flow in fractured media. *International Modeling Center Newsletter* 20, no. 1: 2.

Reynolds, W.D., D.E. Elrick, E.G Youngs, A. Amoozegar, H.W.G. Bootlink, and J. Bouma. 2002. Saturated and field-saturated water flow parameters. In *Methods of Soil Analysis, Part 4: Physical Methods*, 3rd edition, ed. J.H. Dane and G.C. Topp. Madison, Wisconsin: American Society of Agronomy, Soil Science Society of America.

Sheldon, A., 2002. Diffusion of radiogenic helium in shallow ground water: Implications for crustal degassing. Ph.D. dissertation, University of Utah, Department of Geology and Geophysics. Salt Lake City, Utah.

Stute, M., and P. Schlosser. 2001. Atmospheric noble gases. In *Environmental Tracers in Subsurface Hydrology*, ed. P. Cook and A.L. Herczeg. Boston, Massachusetts: Kluwer Academic Publishers.

Sugisaki, R., and K. Taki.1987. Simplified analyses of He, Ne, and Ar dissolved in natural waters. *Geochemical Journal* 21, 21–27.

Tang, J.S., and B.J. Harker. 1991a. Interwell tracer test to determine residual oil saturation in a gas-saturated reservoir, Part 1. Theory and design. *Journal of Canadian Petroleum Technology* 30, no. 3: 76–85.

Tang, J.S., and B.J. Harker. 1991b. Interwell tracer test to determine residual oil saturation in a gas-saturated reservoir, Part 2: Field applications. *Journal of Canadian Petroleum Technology* 30, no. 4: 34–42.

Tang, J.S. 1995. Partitioning tracers and in-situ fluid saturation measurements. *SPE Formation Evaluation* 10, 33–39.

Toride, N., F.J. Leij, and M.T. van Genuchten. 1993. A comprehensive set of analytical solutions for nonequilibrium solute transport with first-order decay and zero-order production. *Water Resources Research* 29, no. 7: 2167–2182.

Toride, N., F.J. Leij, and M.T. van Gnuchten. 1999. The CXTFIT code for estimating transport parameters from laboratory or field tracer experiments, Version 2.1. U.S. Salinity Laboratory Research Report 137.

Vulava, V.M., E.B. Perry, C.S. Romanek, and J.C. Seaman. 2002. Dissolved gases as partitioning tracers for determination of hydrogeological parameters. *Environmental Science & Technology* 36, no. 2: 254–262.

Wood, W.W. 1973. A technique for using porous cups for water sampling at any depth in the unsaturated zone. *Water Resources Research* 9, no. 2: 486–488.